Heliyon 11 (2025) e42622

Contents lists available at ScienceDirect

Heliyon

journal homepage: www.cell.com/heliyon

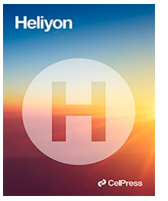

Research article

Spatial patterns of water quality and remote sensing indices from UAV-based multispectral imagery across an irrigation pond

S. Hong [a,b], B.J. Morgan [a], M.D. Stocker [a], J. Smith [c], Y.A. Pachepsky [a,*]

[a] Environmental Microbial and Food Safety Laboratory, USDA-ARS, Beltsville, MD, USA
[b] Department of Civil Urban Earth and Environmental Engineering, Ulsan National Institute of Science and Technology, Ulsan, Republic of Korea
[c] Oak Ridge Institute of Science and Education, Oak Ridge, TN, USA

ARTICLE INFO

Keywords:
Water quality
Unmanned aerial vehicles
Pattern correlation
Remote sensing indices

ABSTRACT

Water quality of irrigation water is an essential factor for public safety and farm sustainability. Imaging surface water sources from unmanned aerial vehicles (UAVs) has become an important source of water quality information. Water quality variables (WQVs) in irrigation ponds have been shown to have persistent spatial patterns. The objective of this work was to test the hypothesis that (a) persistent spatial patterns can be found in reflectance and remote sensing indices from UAV-based multispectral imagery of irrigation ponds, and (b) those patterns can significantly correlate with patterns of WQVs. We utilized data from sampling, in-situ sensing, and UAV-based imaging of a commercial 4-ha farm pond in Maryland. Seventeen water quality variables were measured on a permanent grid during the irrigation season concurrently with the imaging of the pond with the MicaSense RedEdge camera at five wavelengths. Twenty-four remote sensing indices were computed. Spatial patterns were determined using the mean relative difference method. The water quality patterns appeared to reflect differences in distances from banks, closeness to the creek meeting the pond, the degree of water stagnancy, dominant wind directions, and a geese congregation site. High (>0.8) Spearman correlation coefficients were found for turbidity, photosynthetic pigments, and organic carbon in water. These variables' patterns had similarities with patterns of remote sensing indices AFAI, TCARI, TCI, and MCARI. Patterns of *E. coli* strongly correlated with the pattern of reflectance at the red wavelength. Given the high spatiotemporal variability of WQVs in irrigation ponds, determining patterns of remote sensing indices can be useful for the design of surveys or monitoring important aspects of water quality.

1. Introduction

Remote sensing has become a widespread methodology to quantify water quality in surface waters [1,2]. Lakes and reservoirs have been successfully surveyed and monitored [3], lately with the active use of machine learning techniques [4]. Recently, unmanned aerial vehicles (UAVs) have become a source of valuable water quality data. They can provide high-resolution data and support real-time monitoring [5].

It has long been recognized that many environmental variables related to water quality, e.g. chlorophyll content, greenness, vegetation density, turbidity, and dissolved organic matter, may correlate with so-called remote sensing indices, i.e., simple arithmetic

* Corresponding author.
E-mail address: yakov.pachepsky@usda.gov (Y.A. Pachepsky).

https://doi.org/10.1016/j.heliyon.2025.e42622
Received 5 October 2024; Received in revised form 8 February 2025; Accepted 10 February 2025
Available online 11 February 2025

combinations of reflectance measured at two or three wavelengths or wavelength ranges. Many remote sensing indices have been suggested [6,7].

Water quality in irrigation ponds presents substantial interest as a public health factor if this water is used for produce irrigation [8,9], or recreation. Using machine learning, researchers successfully evaluated microbial water quality by *E. coli* concentrations using drone-based imagery of irrigation ponds and identified the most informative water quality parameters with respect to microbial water quality [10,11].

Spatiotemporal variation of environmental variables often demonstrated the presence of persistent spatial patterns [12]. The discovery of such patterns provided valuable information for monitoring design and identifying factors responsible for the presence of hot and cold spots of water quality [13,14]. Well-defined persistent spatial patterns of water quality parameters were found in irrigation ponds [15].

The imagery of water bodies revealed persistent spatial patterns. Such patterns were reported for the remote sensing indexes and were used to assess water quality in surface waters [2,16]. So far, spatial patterns of remote sensing indices have not been studied in the images of irrigation ponds.

We hypothesized that (a) persistent spatial patterns can be found in reflectance and remote sensing index data from UAV-based multispectral imagery of irrigation ponds, and (b) a significant correlation may exist between spatial patterns of water quality variables and patterns of the reflectance and remote sensing indices from imagery across an irrigation pond. This work aimed to test this hypothesis with data from sampling, in-situ sensing, and drone-based imaging of a farm pond in Maryland.

2. Materials and methods

2.1. Sampling, sensing, and imaging at the field site

The research was carried out at a 4-ha commercial irrigation pond in Maryland. Nineteen observation locations (Fig. 1) were selected to reflect various potential factors of water quality conditions, such as preferred area of geese flock presence around location 12, shallowness of nearshore areas locations (11–18), possible bank seepage (location 11), closeness to the stream inlet (location 19), submerged aquatic vegetation (location 1–9), opportunities for the alongshore flow and dead-end low or no-flow areas (locations 14, 15, 16, 17, 18), closeness to the irrigation water intake (locations 10, 18). The pond was surveyed with the autonomous surface vehicle HYCAT (YSI Yellow Springs, OH) in spring before development of the submerged aquatic vegetation to obtain the bathymetry map. The maximum depth of the pond was 2.5 m at the irrigation intake (location 10), with the remainder of the waterbody having a depth of 1–1.5 m with the exception of the area next to the dock (location 3), which had a depth of 2 m, and no sharp changes in the water depth were found across the pond. The pond was visited eight times from June to August 2023.

The multispectral imagery was acquired using a Red Edge-M (MicaSense, Seattle, WA) sensor configuration mounted on a 3DRSolo® (3DR, Berkeley, CA) drone at an altitude of 400 ft (120 m). The multispectral reflectance was obtained at five wavelength bands: blue, green, red, red edge, and near-infrared (NIR) that had 475 nm, 560 nm, 668 nm, 717 nm, and 840 nm as center wavelengths, respectively. The imaging was conducted under clear skies, and the solar zenith angle ranged from 20° to 30°.

A YSI water quality sonde was used to measure pH, dissolved oxygen (DO, mg L^{-1}), specific conductance (SPC, μS cm^{-1}), chlorophyll A (CHL YSI, relative fluorescence units, RFU), phycocyanin (PC YSI, RFU), fluorescent dissolved organic matter (fDOM, μg L^{-1}), water temperature (Temp, °C), turbidity (nephelometric turbidity units, NTU), and location GPS coordinates.

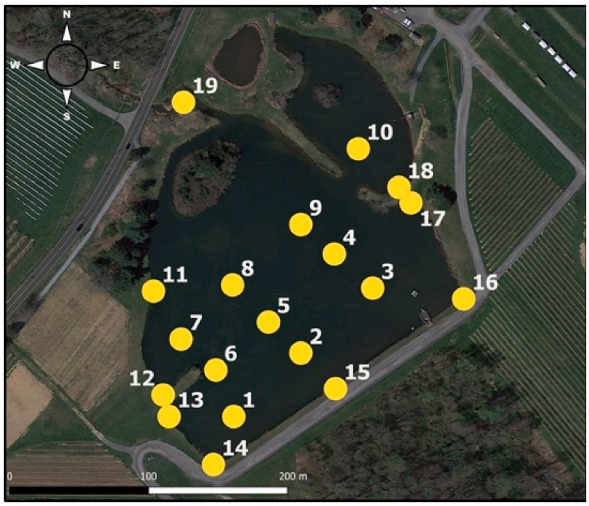

Fig. 1. Locations of sampling, in situ sampling, and imagery data matching at the studied pond.

2.2. Laboratory determinations

Water samples were analyzed using the Aquafluor fluorometer (Turner Designs, San Jose, CA) for colored dissolved organic matter (CDOM, μg/L), whole cell chlorophyll-*a* (CHL_LAB, RFU), and phycocyanin (PC_LAB, μg/L). A Skalar Formacs^{HT} carbon analyzer was utilized to measure water samples total carbon (TC, mg L^{-1}), total organic carbon (TOC, mg L^{-1}), total inorganic carbon (TIC, mg L^{-1}), and total nitrogen (TN, mg L^{-1}) in the water samples. Concentrations of orthophosphate PO_4^{3-} (PO4, mg L^{-1}) and nitrate NO_3^- (NO3, mg L^{-1}) were measured with a SEAL AQ300 discrete nutrient analyzer (Seal Analytical Inc., Mequon, Wisconsin).

2.3. Remote sensing indices

The images were processed with the Pix4D software (Pix4D S.A., Prilly, Switzerland) to obtain reflectance maps for each of the five wavelengths. The statistical distributions of individual pixel reflectance within a 3-m diameter circular buffer area around the water sampling and sensing locations were found normal using the Shapiro-Wilk test at the 0.05 significance level, and the average reflectance values within those areas were used in computations of remote sensing indices which were found to correlate with environmental variables in published applications of the remote sensing imagery in environmental studies. As the indices were originally developed with data from various sensors at various scales; it was not possible to conclude a priori which of them would be efficient with drone-based imagery data of the pond water surface. We computed 24 popular remote sensing indices that have been applied in the past to evaluate presence and status of vegetation (indices EVI, GLI, gNDVI, MSAVI, NDVI, OSAVI, RVI, SAVI, TGI, TVI, NGRDI, TCARI, Combined TCARI, VARI), chlorophyll stock (indices CLI-G, CI-RE, CVI, MCARI, MTCI, NDCI, TCARI, TCI), aquatic

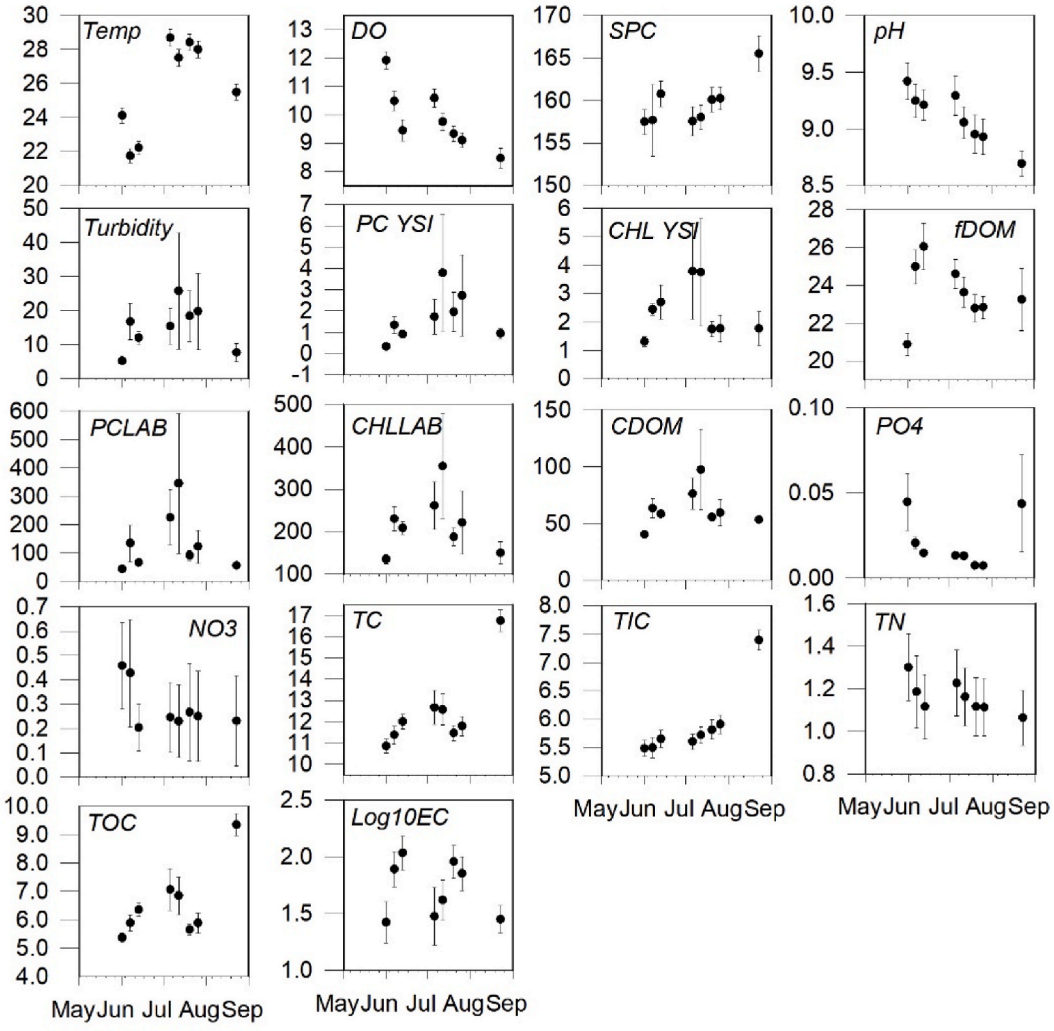

Fig. 2. Average and standard error values of water temperature and water quality variables across the pond sampling locations during the observation period. Measurement units are in the "Materials and Methods" section.

vegetation (indices AFARI and NDAVI), and Turbidity (NDTI). The full names of indices, equations to compute them, and references are in Supplemental Table 1. The indices were selected so that the wavelengths of their development were within the bandwidth ranges of the MicaSense Red Edge imagery.

2.4. Defining spatial patterns

The spatial patterns of water quality and imagery-related variables were determined using relative differences between variable values in individual locations and the average of measurements across all locations [17]. These relative differences were computed after each site visit. At the end of the season, there were eight values of relative difference for each variable at each location. The average of those eight values (mean relative difference or MRD) at each location characterized the tendency of a variable to exceed the

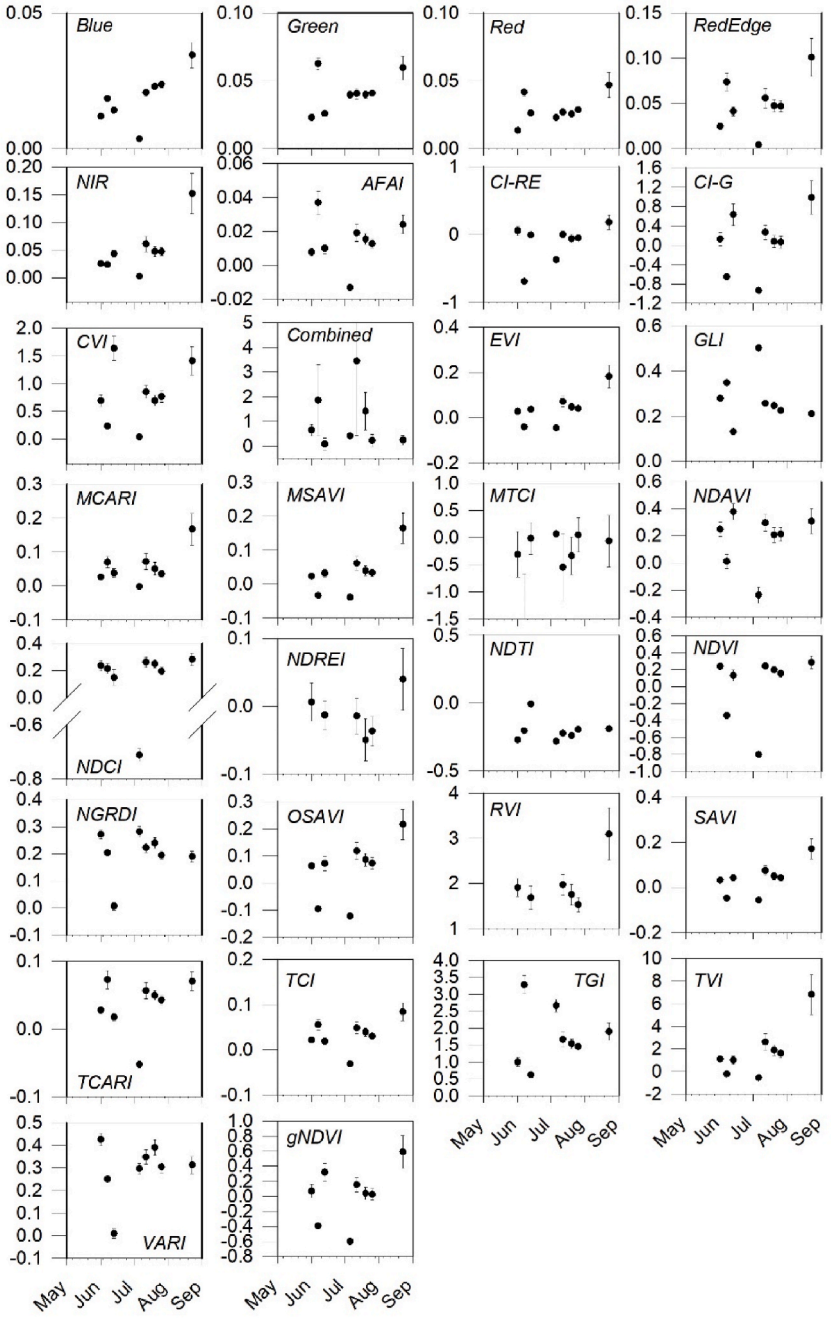

Fig. 3. Averages and standard errors of reflectance and remote sensing indices.

average across the pond or to be smaller than that average. The set of MRD values at all observation locations for each water quality and image-related variable revealed the spatial pattern of this variable across the pond. Equations for the above computations are as follows. Let x_{ij} be the measurement of a variable x made at the location i on jth visit to the site. Relative differences RD_{ij} defined for each location i for a single visit j are:

$$RD_{ij} = \frac{x_{ij} - \overline{x}_j}{\overline{x}_j} \tag{1}$$

where $\overline{x}_j = \frac{1}{N_i} \sum_{i=1}^{i=N_i} x_{ij}$- average across all locations on the jth site visit, N_i is the total number of observation locations of the variable x. The mean relative difference, MRD of the variable x at location i is the mean value of RD_{ij} computed over measurements made over all site visits j,

$$MRD_i = \frac{1}{N_j} \sum_{j=1}^{j=N_j} RD_{ij} \tag{2}$$

where N_j is the total number of site visits. MRD values reflect the pattern in variation of variables over the observation period. Large positive MRDs indicate that the RD values tend to be mostly positive, and the value of the observed variable x_{ij} tends to be mostly larger than the average value $\overline{x}$ across the pond. Large negative MRDs indicate the opposite – value of the observed variable x_{ij} appears to be mostly smaller than the average value $\overline{x}$ across the pond.

The relationships between patterns of the studied variables were characterized by computing the Spearman correlation coefficients between patterns. These relations were not assumed to be linear but rather monotonic, i. e., both tend to increase or tend to decrease.

3. Results and discussion

Both imagery data and WQVs demonstrated rich dynamics over the observation period. Average values of measured water quality parameters are shown in Fig. 2. Water quality demonstrated substantial variation during the observation period. The increase in temperature ranges from 22 to 24 °C in June to 26–28 °C in July was accompanied by an increase in phycocyanin concentration range from 0.50 to 150 to 200–350 μg L^{-1} and chlorophyll concentration range from 150 to 250 to 250–350 RFU. That indicated the development of phytoplankton blooms with the substantial participation of cyanobacteria. Large standard errors of both

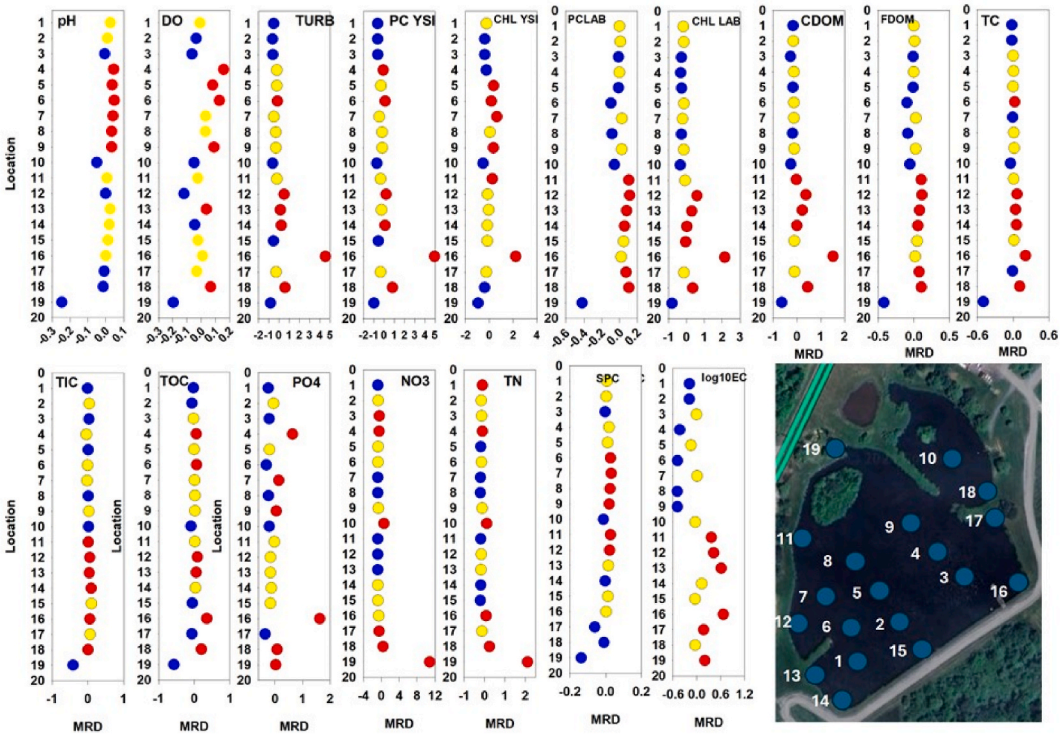

Fig. 4. Spatial patterns of water quality variables. The red fill color is assigned to the top six MRD values corresponding to locations most exceeding the average. The blue fill color is assigned to the bottom MRD values, which are the smallest compared to the average. The yellow fill color is assigned to locations with intermediate MRD values that are close to zero.

photosynthetic pigments indicated the heterogeneous distribution of the bloom across the pond. At the bloom's start, both dissolved oxygen and pH near the water surface experienced an increase, and after this initial increase, an almost linear decrease occurred. The CDOM grew as the bloom started, but its maximum was observed after the bloom had somewhat progressed. Phytoplankton blooms have been found to directly alter CDOM concentrations and can be derived from phytoplankton degradation within water [18]. Dynamics of macronutrient anion concentrations of orthophosphate (PO4) and nitrate (NO3) ions did not reflect changes in CDOM and photosynthetic pigments. The nitrate and total nitrogen variability was very high, while it was low for the orthophosphate PO4. The latter was relatively high (0.05 mg L^{-1})at the beginning of the observation period and was getting smaller from June to July (Fig. 2). Algae and cyanobacteria utilized orthophosphate and nitrate for growth, which agrees with the observations of other authors [19–21].

Total carbon and total organic carbon peaked at the time of the bloom, whereas the total inorganic carbon grew during the observation period, possibly concomitantly with the pH decrease according to the CO_2 dissolution equilibrium. The *E. coli* population grew steadily at the beginning of the observation period but substantially decreased as the presumptive phytoplankton bloom started. The *E. coli* population increased during the time of the phytoplankton bloom but became smaller again in August, and photosynthetic pigment concentrations were low at this time. The overall decrease in chlorophyll and phycocyanin coincided with a decrease in dissolved oxygen and pH, as was repeatedly reported for aquatic environments [22,23]. The increase of total and organic carbon in water indicated the decreasing favorability of conditions for bacteria and phytoplankton, which in turn could indicate the persistent presence of lysed material, including some toxic substances [24]. Increases in the phytoplankton concentrations are often associated with increases in the turbidity of waters which can potentially shield *E. coli* populations from solar irradiation [25,26]. Turbidity became low in the end of the observation period (Fig. 2), and that could negatively affect the *E. coli* survival.

The time dependences of the imagery-related information are shown in Fig. 3. The reflectance and remote sensing indices demonstrated a wide variety of changes during the observation period. Before the phytoplankton bloom, i.e., on the first three observation times, reflectance at blue, green, red, and red-edge wavelengths showed similar behavior, whereas the near-infrared reflectance was approximately constant. Blue and red-edge reflectance became close to zero when the intensive phytoplankton bloom started. As the bloom progressed, the reflectance at all wavelengths stabilized around low values of 0.022, 0.040, 0.027, 0.050 and 0.052 for blue, green, red, red-edge and infra-red wavelengths, respectively. The highest reflectance at all wavelengths was found at the last observation time when the highest average specific conductance of 165 μS cm^{-1} and the highest total organic carbon of 9.4 mg L^{-1} were observed (Fig. 2).

Most remote sensing indices in Fig. 3 responded with sharp change when the phytoplankton bloom started, although the amplitudes of this change varied. Most indices had almost the same values in July, one week or more after the phytoplankton bloom began. Measured by the variation coefficient, most indices' variability was smaller than that of the WQVs. The highest variability for many indices was observed at the last observation time.

Patterns of WQVs computed according to (1) and (2) as the set of MRD values of the observation locations are shown in Fig. 4. Location 19 is notably different from the rest of the sampling locations. It has pH and dissolved oxygen substantially (25 % on average) lower than the rest. The location had the lowest turbidity, CDOM, chlorophyll *a*, and organic carbon concentrations, along with the highest concentrations of nitrate, the lowest SPC, and one of the six highest *E. coli* concentrations relative to the average across the pond. Given that location 19 is close to the place where a small creek meets the pond, it is probable that water quality at location 19 reflects that of the stream water composition rather than the composition typical for the pond itself. In prior research, the differences between water quality at the location where a creek meets a pond and the rest of the pond were noted for two other irrigation ponds in Maryland (Stocker et al., 2021). Another extreme of water quality was found in location 16. This corner location is essentially stagnant, with the stagnancy enhanced by the floating dock, and is on the predominantly leeward side. High MRD values show that location 16 had very high concentrations of fluorescent organic matter and chlorophyll (250 % of average across the pond). Location 10 is close to the intake of irrigation water. Relatively low pH and DO, low carbon and orthophosphate concentrations, and one of the highest

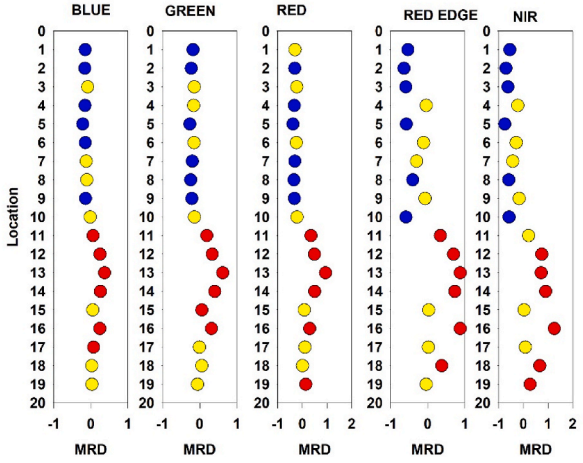

Fig. 5. Spatial patterns of reflectance at five wavelengths at sampling locations.

relative nitrogen concentrations make this location appropriate for irrigation water intake.

Interior locations 1–5 and 7–9 tend to have higher values of pH and DO when compared with nearshore locations (Fig. 4). These locations also have intermediate or low relative concentrations of phycocyanin and chlorophyll, which indicates less favorable conditions for the cyanobacteria bloom compared with the nearshore. Location 6 presents an exception, being set in the interior yet having a large relative difference between turbidity chlorophyll and carbon. However, this location is relatively close to the tip of "micro-peninsula" and that explains why some MRDs are close to some other nearshore location MRD such as 12 or 14. Interestingly, the closeness to the bank does not necessarily affect water quality negatively. Location 15 presents an example with intermediate values of pH and DO, low or intermediate bloom-related values of photosynthetic pigments, organic carbon, and *E. coli*. The alongshore flow prevents the accumulation of phytoplankton and excessive photosynthesis. It has been noted that such conditions are less favorable for accumulation of cyanobacteria [27]. Similarly, at location 17, the MRD of carbon and the MRD of photosynthetic pigments can have significant differences. That may be an artifact related to the availability of only one observation in the after-bloom period in August (Fig. 2), when the decrease in photosynthetic pigments, e.g. chlorophyll down to 50 RFU, was observed along with the increase of dissolved organic carbon from 6.0 to 9.5 mg L^{-1} (Fig. 2). MRD of different water quality parameters have quite different spreads (Fig. 4). Whereas MRD spreads of pH, DO, and SPC are within the range −0.2 to 0.2, spreads of MRD of PC and CHL are much higher, e.g. from −1 to 2 for CHL_LAB, mostly because the data from nearshore and interior samples are pooled together. The highest specific conductance MRD values were found both in the interior (6–9) and nearshore (11 and 12) locations. However, values of SPC MRDs were very low (Fig. 4) and indicated a weak spatial difference of the dissolved solids concentrations in pond water characterized by SPC (Fig. 2).

MRD of reflectance at different wavelengths bears resemblance (Fig. 5). The strongest similarity was obvious between red edge and NIR MRDs. In interior locations 1–9, MRDs are mostly negative, i.e., reflectance is smaller than average reflectance across the pond. The nearshore locations have mostly high positive reflectance MRD. Shallowness of water and related reflection from the bottom, the presence of suspended particles scattering the incoming radiation, and the phytoplankton increase can be reasons for that [28]. A close

	DO	SPC	PH	NTU	PC_YSI	CHL_YSI	FDOM	PC_LAB	CHL_LAB	CDOM	PO4	NO3	TC	TIC	TN	TOC	log10EC
DO	1																
SPC	0.502	1												From	To		
PH	0.756	0.742	1											0.801	1	Vert strong	
NTU	0.377	0.219		1										0.601	0.8	Strong	
PC_YSI	0.484	0.309	0.275	0.925	1									0.401	0.6	Moderate	
CHL_YSI	0.489	0.693	0.609	0.44	0.456	1								0.201	0.4	Fair	
FDOM				0.551	0.377		1							-0.399	-0.2	Fair	
PC_LAB				0.798	0.712		0.712	1						0.599	-0.4	Moderate	
CHL_LAB				0.76	0.649	0.363	0.758	0.8	1					-0.799	-0.6	Strong	
CDOM				0.833	0.721	0.342	0.842	0.904	0.909	1							
PO4				0.246	0.291		0.261	0.289		0.393	1						
NO3		-0.789	-0.565	-0.249	-0.202	-0.651	-0.296		-0.311	-0.225		1					
TC	0.314	0.275		0.856	0.9	0.421	0.514	0.754	0.804	0.789	0.282	-0.249	1				
TIC	-0.356	-0.214	-0.281				0.465	0.46	0.57	0.46			0.395	1			
TN		-0.598	-0.463			-0.507	-0.218					0.774		-0.319	1		
TOC	0.498	0.409	0.314	0.902	0.954	0.447	0.361	0.682	0.621	0.686	0.337	-0.288	0.889			1	
log10EC	-0.5	-0.27	-0.549	0.333			0.496	0.372	0.44	0.47	0.218			0.314			1
Blue	-0.442	-0.225	-0.512	0.44	0.26		0.588	0.537	0.593	0.607			0.475	0.567		0.244	0.802
Green	-0.356	-0.226	-0.465	0.523	0.311		0.614	0.67	0.661	0.679			0.521	0.479		0.33	0.789
Red	-0.5	-0.267	-0.539	0.4			0.567	0.532	0.607	0.574			0.381	0.46			0.849
RedEdge				0.767	0.64	0.242	0.656	0.788	0.754	0.867	0.382		0.73	0.349		0.616	0.614
NIR			-0.312	0.658	0.535		0.602	0.737	0.693	0.788	0.404		0.632	0.319		0.509	0.675
AFAI	0.27	0.298		0.835	0.774	0.472	0.612	0.789	0.749	0.872	0.44	-0.309	0.811	0.296		0.76	0.433
CI-RE	-0.626	-0.702	-0.753			-0.509		0.365	0.233	0.226	0.244	0.546		0.402	0.505		0.432
CI-G		-0.204	-0.389	0.565	0.454		0.474	0.553	0.632	0.665	0.302		0.518			0.423	0.626
CVI		-0.221	-0.404	0.56	0.482		0.493	0.626	0.581	0.684	0.419		0.539	0.211	0.274	0.432	0.616
Combine					-0.202		0.221						-0.326				
EVI			-0.304	0.672	0.57		0.621	0.732	0.704	0.811	0.437		0.637	0.277		0.523	0.614
GLI	0.544	0.386	0.73				-0.351	-0.251	-0.372	-0.358				-0.412			-0.756
MCARI	0.246			0.828	0.791	0.374	0.579	0.809	0.728	0.856	0.46		0.818	0.274		0.76	0.421
MSAVI			-0.296	0.686	0.593		0.598	0.733	0.709	0.807	0.407		0.663	0.281		0.547	0.598
MTCI	-0.34			-0.423	-0.395		-0.46	-0.514	-0.365	-0.479	-0.214		-0.439	-0.246		-0.318	
MTVI2	-0.218		-0.245	-0.291	-0.2								-0.2	-0.373	0.464		0.364
NDAVI				0.688	0.57		0.633	0.77	0.616	0.782	0.419		0.611	0.256		0.553	0.537
NDCI	0.489	0.344	0.228	0.767	0.805	0.414	0.496	0.709	0.521	0.754	0.579		0.716			0.781	
NDREI		-0.212	-0.26						0.218		-0.258						
NDTI	0.639	0.614	0.861			0.325	-0.351	-0.302	-0.372	-0.333		-0.372		-0.333	-0.323		-0.765
NDVI			-0.318	0.625	0.554		0.577	0.67	0.609	0.746	0.484		0.574		0.282	0.512	0.602
NGRDI	0.639	0.614	0.861			0.325	-0.351	-0.302	-0.372	-0.333		-0.372		-0.333	-0.323		-0.765
OSAVI			-0.302	0.675	0.584		0.612	0.721	0.698	0.807	0.439		0.651	0.286		0.533	0.605
RVI			-0.286	0.63	0.605		0.518	0.719	0.568	0.725	0.498		0.605		0.351	0.539	0.453
SAVI			-0.302	0.675	0.584		0.612	0.721	0.698	0.807	0.439		0.651	0.286		0.533	0.605
TCARI	0.221			0.854	0.761	0.396	0.674	0.825	0.76	0.907	0.43	-0.254	0.793	0.314		0.74	0.505
TCI	0.265	0.202		0.853	0.791	0.398	0.623	0.814	0.767	0.888	0.454	-0.212	0.833	0.275		0.772	0.451
TGI				0.721	0.572	0.261	0.661	0.802	0.809	0.802		-0.309	0.753	0.414		0.642	0.479
TVI			-0.326	0.456	0.337		0.472	0.467	0.604	0.614	0.226		0.495	0.265		0.34	0.684
VARI	0.626	0.619	0.854			0.337	-0.358	-0.321	-0.368	-0.344		-0.393		-0.321	-0.344		-0.77
gNDVI			-0.404	0.568	0.467		0.467	0.558	0.633	0.66	0.277		0.528			0.435	0.614
	DO	SPC	PH	NTU	PC_YSI	CHL_YSI	FDOM	PC_LAB	CHL_LAB	CDOM	PO4	NO3	TC	TIC	TN	TOC	log10EC

Fig. 6. Spearman correlations between patterns of WQVs and imagery information, including reflectance and remote sensing indices. Very strong correlations are often found with TCI and MCARI (4 instances each) and TCARI and TGI (3 instances each). Strong correlations are found with MRD of Red Edge (9 instances), TCARI (8 instances), NIR, AFAI, EVI, and MCARI (7 instances each), and NDAVI (6 instances).

to zero reflectance MRD (except green wavelength) was observed at location 15, turbidity was on average the lowest of all other pond locations (Fig. 4). The highest reflectance MRD are found in locations 13 and 16, where obvious phytoplankton bloom development and later accumulation of carbon tended to occur (Fig. 4). Strong similarity was obvious between red and NIR MRDs. Location 19, although it had water quality properties different from the rest of the pond, did not demonstrate low reflectance. The spread of MRD values was relatively high and varied between 1 and 2. That spread increased with the wavelength.

Fig. 6 shows the Spearman correlation coefficients r_s between MRDs of the remote sensing indices and water quality parameters at the same locations. High correlations indicate the similarity of deviations from averages. The correlations are significant at the 0.05 level of significance if the r_s are larger than 0.45. Table 1 shows the indices, MRD of which have the highest and the second highest Spearman correlations with MRDs of water quality variables. Of the most highly correlated index patterns, only AFAI and NDTI were developed for aquatic systems. AFAI was recently proposed and used to estimate the fractional coverage of floating algae, chlorophyll content, and phytoplankton blooms from satellite imagery [29–31]. The NDTI was introduced to estimate turbidity in water bodies with satellite information and UAV imagery [32,33]. Interestingly, the NDTI pattern was not correlated with the turbidity pattern in this work possibly because turbidity in the pond substantially differed from turbidity in other water bodies by its source, for example, due to formation of reactive oxygen species damaging phytoplankton cells [34].

The highest correlations are with WQVs reflecting phytoplankton activity and carbon in water. The patterns of these variables are similar to those of AFAI, TCARI, and TCI. The MCARI index has values close to the strong correlation threshold set at 0.8. Other indices with patterns correlating with water quality patterns were not developed for and were very rarely applied in aquatic environments' TCARI index was developed and used to assess plant stresses [35], especially water stress and stresses related to disease and heat. The index is actively used with UAV data [36]. It was designed to reflect the changes in chlorophyll content as water stress progressed [37]. In the studied pond, the pattern TCARI correlated with CDOM and phycocyanin patterns. The TCI remote sensing index had patterns similar to organic and total carbon. The purpose of this index is the same as that of TCARI. And their patterns were almost identical with the Spearman correlation of 0.982. Overall, the correlation of the WQV patterns with patterns of indices developed both for aquatic and terrestrial systems supports the observation of lakes in Peru using vegetation indices developed for terrestrial systems [38]. Authors concluded that such indices can be used to detect and analyze the dynamics of biological beings with photosynthetic activity in aquatic ecosystems.

Patterns of chlorophyll in water samples (CHLLAB) did not resemble patterns of chlorophyll obtained with the YSI. The vertical scale mismatch may be a possible reason for that. The YSI sensor provides the average information along the sensor length. High chlorophyll concentrations are near the surface, and those concentrations nonlinearly decrease with depth. This can be most pronounced for cyanobacteria, some of which might have gas vacuoles controlling their vertical movements. Therefore, averages of those nonlinear dependencies may not change spatially in the same way as in the thin surface layer sensed by imaging. It appeared that the patterns of red and blue reflectance correlate very strongly with the patterns of *E. coli*. This is quite an interesting fact given the importance of *E. coli* as the microbial quality indicator organism and the resource- and time-consuming current methods of its determination. It appears worthwhile to research if the microbial quality of irrigation water assessment may be expedited (or supplemented) by the use of UAVs.

Relationships between the water quality patterns and imagery data can be useful to guide the monitoring or survey design. Substantial variability of water quality parameters indicates the need to design the water quality monitoring according to the intended use of water. If recreational activities are of interest, the nearshore samples should be collected, whereas the pond interior should be sampled if the water is planned to be used for irrigation. However, even among the nearshore samples as well as among the interior samples, the variability of water quality may be quite high (Fig. 5). Therefore, using patterns of indices correlating with patterns of

Table 1
Remote sensing indices and/or wavelengths, MRD of which have the highest correlations with MRD of WQVs.

Water quality variable	The highest correlation	r_s	Second highest correlation	r_s
	Spectral index or wavelength		Spectral index or wavelength	
DO	NDTI	0.639	CL-RE	0.626
SPC	CL-RE	−0.702	VARI	0.619
PH	NDTI	**0.861**	CL-RE	−0.763
TURB	AFAI	**0.835**	MCARI	**0.828**
PCYSI	NDCI	**0.805**	MCARI	0.791
CHLYSI	AFAI	*0.472*	CL-RE	*−0.509*
FDOM	TCARI	0.674	TGI[¶]	0.661
PCLAB	TCARI	**0.825**	TCI	**0.814**
CHLLAB	TGI	**0.809**	MCARI	0.728
CDOM	TCARI	**0.907**	AFAI	**0.872**
PO4	NDCI	*0.579*	RVI	*0.498*
NO3	CL-RE	*0.546*	NS	
TN	CL-RE	*0.505*	NS	
TIC	BLUE	*0.567*	GREEN	*0.469*
TOC	NDCI	0.781	TCI	0.772
TC	TCI	**0.833**	AFAI	**0.811**
ECMPN	RED	**0.849**	BLUE	**0.802**

Bold – very strong, regular – strong, italics – moderate correlation, NS = Not Significant.

water quality may be beneficial by providing the distinction between different locations caused by local conditions such as water movement or nutrient source.

The indices with patterns best related to the patterns of WQVs in this work have been developed both for aquatic systems, i.e., alternate floating algae index (AFAI), and for terrestrial ecosystems, i.e. triangular greenness index (TCI), transformed chlorophyll adsorption reflectance index (TCARI), and chlorophyll index – red-edge (CL-RE). Other indices developed for aquatic systems, i.e., normalized difference aquatic vegetation index (NDAVI) or normalized difference turbidity index (NDTI), did not make it to Table 1 but also had tight relationships of their patterns with patterns of WQVs. For example, the NDTI pattern had a strong relationship with the pattern of *E. coli* (Fig. 6).

It needs to be noted that the remote sensing indices were developed to correlate measured values of WQVs and values of indices rather than the spatial patterns of these data. The analysis in this work aims to compare the spatial trends rather than the values themselves. The Spearman correlation coefficients do not reflect indices' predictive capacity but rather indicate zones where relatively large or relatively small WQV values can be expected.

4. Conclusions

We have reported the results of concurrent measurements of 17 water quality variables and 24 multispectral indices derived from a commercial irrigation pond's multispectral (5 bands) UAV-based imaging. The data analysis showed the following.

- Both water quality variables and remote sensing indices exhibited persistent spatial patterns of relative differences between local values and average values across the pond for each visit.
- Mean relative differences over the observation period reflected water quality factors, such as proximity to the bank, presence of animal waste, and water flow and depth.
- The mean relative differences of most water quality variables were mostly positive in the near shore area and mostly negative in the pond's interior.
- Strong correlations between water quality patterns and some of the remote sensing indices were observed. When established, such correlations can inform about water quality patterns and guide sampling and sensing variables for survey or water quality monitoring and surveys.

This paper reports pilot project results that indicate the opportunities in looking for the best water quality pattern predictors and develop indices specific for an irrigation pond imaged from UAVs. Developments in these directions are expected with the advent of the new generations of hyperspectral cameras, WQV sensors, and unmanned surface vehicles.

CRediT authorship contribution statement

S. Hong: Writing – review & editing, Methodology, Formal analysis, Conceptualization. **B.J. Morgan:** Visualization, Methodology, Investigation, Data curation. **M.D. Stocker:** Methodology, Investigation, Data curation. **J. Smith:** Writing – review & editing, Investigation, Data curation. **Y.A. Pachepsky:** Writing – original draft, Project administration, Funding acquisition, Conceptualization.

Institutional review board statement

Not applicable.

Data availability statement

The raw data supporting the conclusions of this article will be made available by the authors upon request.

Declaration of generative AI and AI-assisted technologies in the writing process

The generative AI were not, and AI-assisted technologies were not used during the preparation of the manuscript.

Funding

Funding for this research was provided by USDA-ARS project 8042-42610-001-000-D.

Declaration of competing interest

The authors declare that they have no known competing financial interests or personal relationships that could have appeared to influence the work reported in this paper.

Appendix A. Supplementary data

Supplementary data to this article can be found online at https://doi.org/10.1016/j.heliyon.2025.e42622.

References

[1] I. Chawla, L. Karthikeyan, A.K. Mishra, A review of remote sensing applications for water security: quantity, quality, and extremes, J. Hydrol. 585 (2020) 124826.
[2] V. Sagan, K.T. Peterson, M. Maimaitijiang, P. Sidike, J. Sloan, B.A. Greeling, S. Maalouf, C. Adams, Monitoring inland water quality using remote sensing: potential and limitations of spectral indices, bio-optical simulations, machine learning, and cloud computing, Earth Sci. Rev. 205 (2020) 103187.
[3] K. Xia, T. Wu, X. Li, S. Wang, H. Tang, Y. Zu, Y. Yang, A new model for assessing water quality status using MODIS images: a case study of large lakes and reservoirs in China, J. Hydrol. (2024) 131545.
[4] J. Ren, H. Zhou, Z. Tao, L. Ge, K. Song, S. Xu, Y. Li, L. Zhang, X. Zhang, S. Li, Long-term monitoring chlorophyll-a concentration using HJ-1 A/B imagery and machine learning algorithms in typical lakes, a cold semi-arid region, Opt. Express 32 (9) (2024) 16371–16397.
[5] B. Choi, J. Lee, B. Park, L. Sungjong, A study of cyanobacterial bloom monitoring using unmanned aerial vehicles, spectral indices, and image processing techniques, Heliyon 9 (5) (2023) e16343.
[6] D. Montero, C. Aybar, M.D. Mahecha, F. Martinuzzi, M. Söchting, S. Wieneke, A standardized catalogue of spectral indices to advance the use of remote sensing in Earth system research, Sci. Data 10 (1) (2023) 1–20.
[7] H. Verena, B. Katharina, Index DataBase. https://www.indexdatabase.de, 2024.
[8] A. Allende, J. Monaghan, Irrigation water quality for leafy crops: a perspective of risks and potential solutions, Int. J. Environ. Res. Publ. Health 12 (7) (2015) 7457–7477.
[9] M. Uyttendaele, L.A. Jaykus, P. Amoah, A. Chiodini, D. Cunliffe, L. Jacxsens, K. Holvoet, L. Korsten, M. Lau, P. McClure, Microbial hazards in irrigation water: standards, norms, and testing to manage use of water in fresh produce primary production, Compr. Rev. Food Sci. Food Saf. 14 (4) (2015) 336–356.
[10] S.M. Hong, B.J. Morgan, M.D. Stocker, J.E. Smith, M.S. Kim, K.H. Cho, Y.A. Pachepsky, Using machine learning models to estimate Escherichia coli concentration in an irrigation pond from water quality and drone-based RGB imagery data, Water Res. (2024) 121861.
[11] B.J. Morgan, M.D. Stocker, J. Valdes-Abellan, M.S. Kim, Y. Pachepsky, Drone-based imaging to assess the microbial water quality in an irrigation pond: a pilot study, Sci. Total Environ. 716 (2020) 135757.
[12] H. Vereecken, Y. Pachepsky, C. Simmer, J. Rihani, A. Kunoth, W. Korres, A. Graf, H.-H. Franssen, I. Thiele-Eich, Y. Shao, On the role of patterns in understanding the functioning of soil-vegetation-atmosphere systems, J. Hydrol. 542 (2016) 63–86.
[13] W.D. Alberto, D.M. del Pilar, A.M. Valeria, P.S. Fabiana, H.A. Cecilia, B.M. de Los Ángeles, Pattern recognition techniques for the evaluation of spatial and temporal variations in water quality. a case study:: suquıa River Basin (Cordoba–Argentina), Water Res. 35 (12) (2001) 2881–2894.
[14] S. Behmel, M. Damour, R. Ludwig, M. Rodriguez, Water quality monitoring strategies—a review and future perspectives, Sci. Total Environ. 571 (2016) 1312–1329.
[15] M.D. Stocker, Y.A. Pachepsky, J. Smith, B. Morgan, R.L. Hill, M.S. Kim, Persistent patterns of *E. coli* concentrations in two irrigation ponds from 3 years of monitoring, Water, Air, Soil Pollut. 232 (2021) 1–15.
[16] P. Bierman, M. Lewis, B. Ostendorf, J. Tanner, A review of methods for analysing spatial and temporal patterns in coastal water quality, Ecol. Indic. 11 (1) (2011) 103–114.
[17] Y. Pachepsky, R. Kierzewski, M. Stocker, K. Sellner, W. Mulbry, H. Lee, M. Kim, Temporal stability of Escherichia coli concentrations in waters of two irrigation ponds in Maryland, Appl. Environ. Microbiol. 84 (3) (2018) e01876-17.
[18] Y. Zhou, E. Jeppesen, Y. Zhang, C. Niu, K. Shi, X. Liu, G. Zhu, B. Qin, Chromophoric dissolved organic matter of black waters in a highly eutrophic Chinese lake: freshly produced from algal scums? J. Hazard Mater. 299 (2015) 222–230.
[19] X. Chen, L. Yang, L. Xiao, A. Miao, B. Xi, Nitrogen removal by denitrification during cyanobacterial bloom in Lake Taihu, J. Freshw. Ecol. 27 (2) (2012) 243–258.
[20] A.M. Gaffney, S.A. Markov, M. Gunasekaran, Utilization of cyanobacteria in photobioreactors for orthophosphate removal from. Twenty-Second Symposium on Biotechnology for Fuels and Chemicals, Humana Press, 2001, pp. 185–193.
[21] A. Vazirzadeh, K. Jafarifard, A. Ajdari, Y. Chisti, Removal of nitrate and phosphate from simulated agricultural runoff water by Chlorella vulgaris, Sci. Total Environ. 802 (2022) 149988.
[22] W. Cao, J. Huan, C. Liu, Y. Qin, F. Wu, A combined model of dissolved oxygen prediction in the pond based on multiple-factor analysis and multi-scale feature extraction, Aquac. Eng. 84 (2019) 50–59.
[23] C. Zang, S. Huang, M. Wu, S. Du, M. Scholz, F. Gao, C. Lin, Y. Guo, Y. Dong, Comparison of relationships between pH, dissolved oxygen and chlorophyll a for aquaculture and non-aquaculture waters, Water, Air, Soil Pollut. 219 (2011) 157–174.
[24] M. Leloup, R. Nicolau, V. Pallier, C. Yéprémian, G. Feuillade-Cathalifaud, Organic matter produced by algae and cyanobacteria: quantitative and qualitative characterization, J. Environ. Sci. 25 (6) (2013) 1089–1097.
[25] L.L. Yuan, Continental-scale effects of phytoplankton and non-phytoplankton turbidity on macrophyte occurrence in shallow lakes, Aquat. Sci. 83 (1) (2021) 14.
[26] K. Zolfaghari, G. Wilkes, S. Bird, D. Ellis, K. Pintar, N. Gottschall, H. McNairn, D. Lapen, Chlorophyll-a, dissolved organic carbon, turbidity and other variables of ecological importance in river basins in southern Ontario and British Columbia, Canada, Environ. Monit. Assess. 192 (2020) 1–16.
[27] S. Merel, D. Walker, R. Chicana, S. Snyder, E. Baurès, O. Thomas, State of knowledge and concerns on cyanobacterial blooms and cyanotoxins, Environ. Int. 59 (2013) 303–327.
[28] U.o. Minnesota, Reflectance spectra of water bodies depend on their dominant optical constituents: implications for satellite sensing of water quality constituents, Retrieved December 26, 2024 from, https://water.rs.umn.edu/spectra, 2024.
[29] M. Cao, S. Qing, E. Jin, Y. Hao, W. Zhao, A spectral index for the detection of algal blooms using Sentinel-2 Multispectral Instrument (MSI) imagery: a case study of Hulun Lake, China, Int. J. Rem. Sens. 42 (12) (2021) 4514–4535.
[30] J. Descloitres, A. Minghelli, F. Steinmetz, C. Chevalier, M. Chami, L. Berline, Revisited estimation of moderate resolution sargassum fractional coverage using decametric satellite data (s2-msi), Remote Sens. 13 (24) (2021) 5106.
[31] Y. Guo, X. Wei, Z. Huang, H. Li, R. Ma, Z. Cao, M. Shen, K. Xue, Retrievals of chlorophyll-a from GOCI and GOCI-II data in optically complex lakes, Remote Sens. 15 (19) (2023) 4886.
[32] K. Ehmann, C. Kelleher, L.E. Condon, Monitoring turbidity from above: deploying small unoccupied aerial vehicles to image in-stream turbidity, Hydrol. Process. 33 (6) (2019) 1013–1021.
[33] V. Garg, S.P. Aggarwal, P. Chauhan, Changes in turbidity along Ganga River using Sentinel-2 satellite data during lockdown associated with COVID-19, Geomatics Nat. Hazards Risk 11 (1) (2020) 1175–1195.
[34] K.H. Cho, J. Wolny, J.A. Kase, T. Unno, Y. Pachepsky, Interactions of *E. coli* with algae and aquatic vegetation in natural waters, Water Res. 209 (2022) 117952.
[35] J. Liu, E. Pattey, J.R. Miller, H. McNairn, A. Smith, B. Hu, Estimating crop stresses, aboveground dry biomass and yield of corn using multi-temporal optical data combined with a radiation use efficiency model, Rem. Sens. Environ. 114 (6) (2010) 1167–1177.

[36] A.d.S. Lopes, A.S.d. Andrade, E.A. Bastos, C.A.d. Sousa, R.A.d.C. Casari, M.S.d. Moura, Assessment of maize hybrid water status using aerial images from an unmanned aerial vehicle, Revista Caatinga 37 (2024) e11701.
[37] D. Haboudane, J.R. Miller, N. Tremblay, P.J. Zarco-Tejada, L. Dextraze, Integrated narrow-band vegetation indices for prediction of crop chlorophyll content for application to precision agriculture, Rem. Sens. Environ. 81 (2–3) (2002) 416–426.
[38] J. Veneros, S. Chavez, M. Oliva, E. Arellanos, J.L. Maicelo, L. García, Comparing six vegetation indexes between aquatic ecosystems using a multispectral camera and a Parrot Disco-Pro Ag Drone, the ArcGIS, and the family error rate: a case study of the Peruvian Jalca, Water 15 (17) (2023) 3103.